IEEE Photonics Journal
An IEEE Photonics Society Publication

A Multipurpose and Highly-Compact Plasmonic Filter Based on Metal-Insulator-Metal Waveguides

Volume 12, Number 3, March 2020

Seyed Morteza Ebadi, ***Student Member, IEEE***
Jonas Örtegren
Mohammad Sajjad Bayati
Siamak Bonyadi Ram

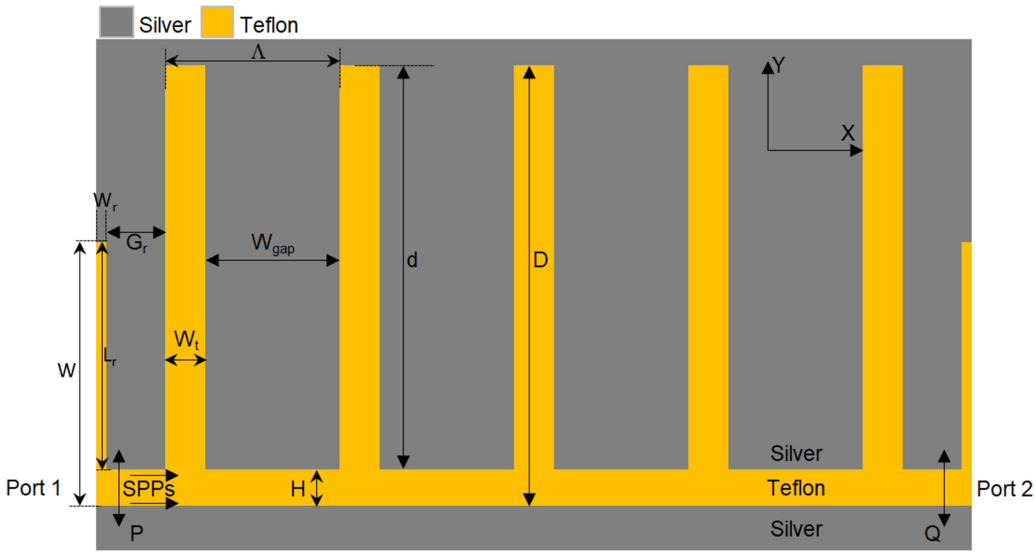

DOI: 10.1109/JPHOT.2020.2974959

A Multipurpose and Highly-Compact Plasmonic Filter Based on Metal-Insulator-Metal Waveguides

Seyed Morteza Ebadi,[1] ***Student Member, IEEE***, **Jonas Örtegren**,[2] **Mohammad Sajjad Bayati**,[3] **and Siamak Bonyadi Ram**[4]

[1]Department of Electronics Design, Mid Sweden University, SE-85170 Sundsvall, Sweden
[2]Department of Natural Sciences, Mid Sweden University, SE-85170 Sundsvall, Sweden
[3]Department of Electrical Engineering, School of Engineering, Razi University, 67149-67346 Kermanshah, Iran
[4]British Columbia Institute of Technology, Burnaby, BC V5G 3H2, Canada

DOI:10.1109/JPHOT.2020.2974959

Manuscript received January 23, 2020; revised February 14, 2020; accepted February 15, 2020. Date of publication February 19, 2020; date of current version April 28, 2020. Corresponding author: Seyed Morteza Ebadi (e-mail: seyed-morteza.ebadi@miun.se.)

Abstract: A multipurpose and ultra-compact nanoplasmonic wavelength filter based on stub structure in a metal-insulator-metal (MIM) waveguide is suggested and numerically investigated. A novel approach of connecting two stepped-like apertures to both input and output ports is applied to form Fabry-Perot (FP) cavities, which enabled the structure to act as a dual band-pass filter at wavelengths 1310 nm and 1550 nm. It is shown that the variation in cavities' length allows to realize a long-wavelength cutoff filter, and cutoff wavelength can be easily tuned by adjusting the length of the cavities. Furthermore, it is revealed that increasing the gap between the stepped-like apertures and the cavities provides a triple band-pass at telecom wavelengths, e.g., 1267.5 nm, 1414.19 nm, and 1644.7 nm. The tunable broadband high-pass wavelength filter is then achieved while the lengths of stepped-like apertures and stub resonators are set to be identical. Finally, a tunable nearly perfect absorber can be obtained by varying the width of stub resonators. Therefore, because of functionality, size, as well as efficiency the proposed plasmonic filter may greatly contribute to miniaturization of next generation of photonic integrated circuits (PICs), and find applications in on-chip integration and wavelength-division multiplexing (WDM) in optical communication systems.

Index Terms: Coupled resonators, Fabry-Perot (FP), optical filters, photonic integrated circuits, surface plasmon polaritons, wavelength filtering devices.

1. Introduction

Surface Plasmon Polaritons (SPPs), are electromagnetic waves propagating at the interface of a metal and dielectric coupled to free electrons of plasma, giving rise to confinement of surface plasmons to the metallic surface with exponentially decaying fields at both mediums [1]–[3]. SPPs-based devices, thanks to their unique features such as overcoming the diffraction limit, guiding and confining light at subwavelength scales, as well as the ability to carry and propagate both optical and electrical signals, provide a promising platform for development of next generation of photonic integrated circuits (PICs), which are ultra-compact and highly energy-efficient. As a result, a considerable number of research studies over the past decade has been devoted to investigate potential applications of plasmonic-based structures such as sensors and biosensors [4], [5],

modulators [6], field-effect transistors (FETs) [7], splitters [8], light absorbers [9], [10] and so forth. In general, there are two distinct types of plasmonic waveguides, namely insulator-metal-insulator (IMI) and metal-insulator-metal (MIM). Unlike the IMI structures that exhibit less propagation loss with low mode confinement, the MIM devices offer strong light confinement with acceptable propagation loss, which make them suitable and attractive for on-chip integration into PICs [11]. Among miscellaneous components, optical filters, which are employed to selectively transmit light in a specific wavelength while rejecting others, play a key role in machine vision systems, fluorescent microscopy, wavelength division multiplexing (WDM) and dispersion compensation. Therefore, a variety of plasmonic filters based on MIM waveguides including band-stop [12]–[14], ring resonators [15], [16], band-pass [17], [18], Fabry-Perot cavity [19], and multi-channel filters [20] are suggested.

Recently, there has been a growing interest in development of multipurpose and multifunctional optical circuits that can perform several functions with a single structure. Due to the fact that designing a multipurpose device is a complex procedure [21], only a few attempts to accomplish such a goal have been made. Wang *et al.* [13] proposed a tunable plasmonic band-stop filter with a cascaded symmetrical stub structure, and achieved a wider band-stop spectrum with increasing number of stubs, and did also study the effect of different lengths of the stubs. Zhuang *et al.* [22] included three stubs in a plasmonic waveguide structure and showed that by tuning the distance between the stubs, the band-stop can be shifted towards longer or shorter wavelengths. Li and Jiao [12] simulated a two-stub MIM plasmonic filter to yield a band-stop filter in the near infrared range. In this work, a plasmonic bandpass filter working at the wavelengths 1310 nm and 1550 nm was designed by using a five-stub structure and through adding stepped-like apertures to both input and output ports. It is shown that the transmission spectrum of the device can be tuned to have different functionalities, including cut-off, triple band-pass, high pass, and a nearly perfect absorber at technologically important optical channels. The realization of such a multipurpose plasmonic device would offer a shortcut path to advancement of condensed optical circuits, while maintaining a high level of efficiency. Compared to similar research studies that offer a single functionality, for example, mostly as a band-stop filter based on stub configurations, our novel proposed plasmonic wavelength filter device not only incorporates several advantages such as comparatively low complexity, shrinking down the size of optical component, and as a suitable candidate for on-chip integration, but it is also enabling realization of multifunctionalities (such as a dual band-pass-, long-wavelength cutoff-, triple band-pass-, and high-pass filter, beside a narrow-band nearly perfect absorber at telecom wavelengths), providing more degrees of freedom to tailor and control the properties of the nanostructure that would play a major role in development of next generation of PICs.

2. Structure Design and Simulations

Fig. 1(a) shows the schematic configuration of a symmetric stub resonator containing five identical stubs. The structure consists of two layers of silver, whose complex permittivity has been taken from the tabulated data of Johnson and Christy [23] and a layer of Teflon, with a refractive index of 1.37, as insulator. Teflon was chosen since it was experimentally demonstrated that Teflon can also be used as a low-dielectric material for integration into semiconductor industry, making it an attractive candidate for CMOS compatible plasmonic waveguide systems [24]. Furthermore, it was later shown that Teflon as a dielectric buffer layer in Kretschmann configuration helps to excite long range surface plasmon resonance, leading to substantial enhancement in the quality factor in, for instance, biomedical applications, as well as assisting to improve fluorescence detection efficiency [25]. Throughout this paper, simulations were carried out by a 3D commercial EM software tool, CST MWS, with frequency domain solver that uses finite element method (FEM) to investigate the performance of the proposed structure. The software solves the Maxwell equations without taking quantum effects into consideration. The following considerations have been taken into account in order to obtain the numerical results in this paper. The width of the waveguide is chosen to be much

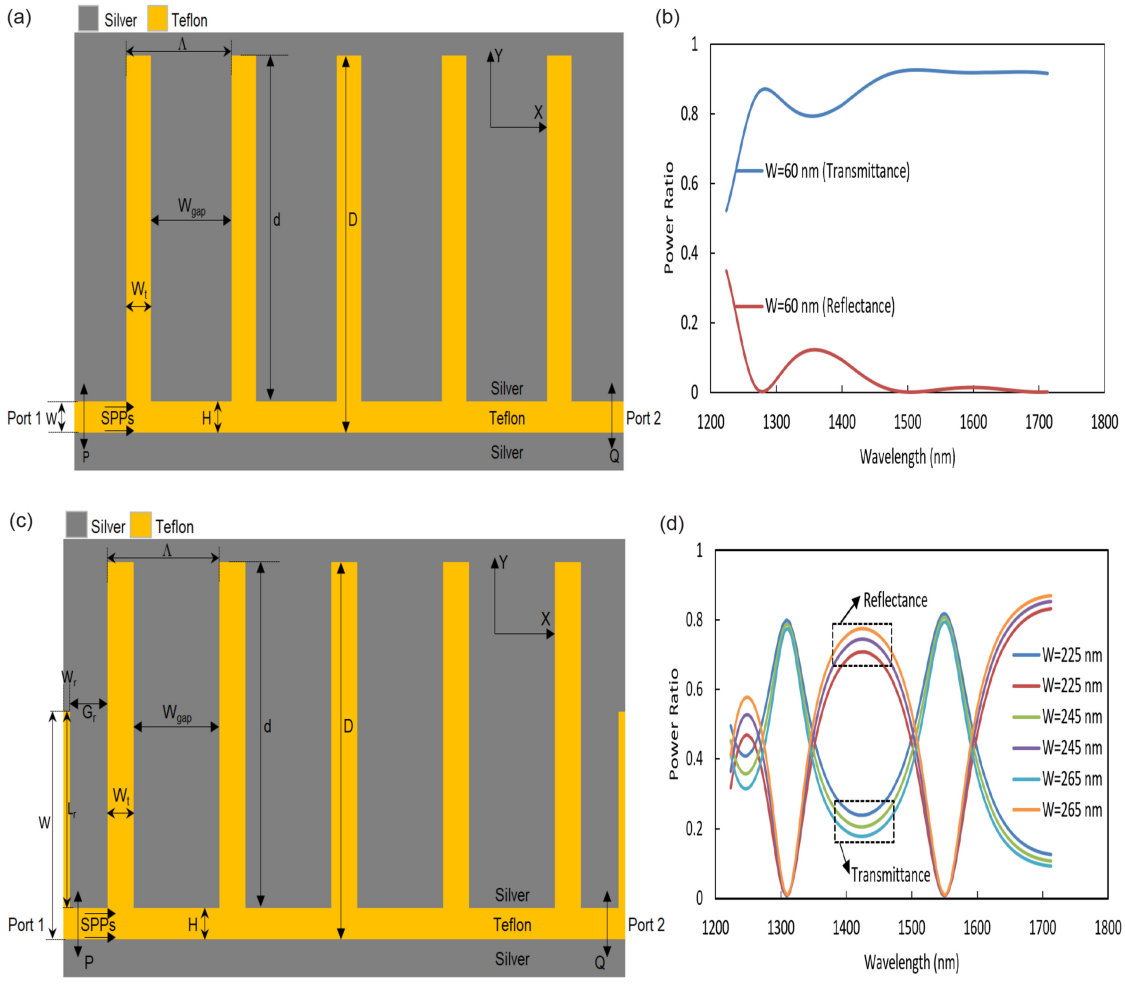

Fig. 1. (a) Schematic of the initial MIM plasmonic waveguide under study. (b) Simulation of transmission and reflection spectrum of the structure with $W = W_t = H = 60$ nm, $d = 400$ nm, $D = d + H = 460$ nm, $W_{gap} = 130$ nm and $\wedge = W_{gap} + W_t = 190$ nm. (c) Schematic illustration of the proposed multipurpose plasmonic filter. (d) Simulation of transmittance and reflectance spectra for $W = 225$ nm, 245 nm, and 265 nm with $W_r = 10$ nm, $L_r = 180$ nm and $G_r = 45$ nm.

smaller than that of the incident wavelength λ, ensuring that only the fundamental TM mode can exist in the structure, which is excited by a dipole source. The grid sizes are chosen to be 5 nm $\times$ 5 nm along the x and y directions. Two power monitors P and Q, respectively, are located at the equal distance from the central waveguide to detect the incident and transmission power. The transmittance is defined to be $T = \frac{P_{out}}{P_{in}}$. In the description of the MIM waveguide, β is the propagation constant achieved by solving the dispersion equation $\varepsilon_{in} k_{z_2} + \varepsilon_m k_{z_1} \tanh(-\frac{ik_{z_1}}{2}\omega) = 0$. Here k_{z_1} and k_{z_2} are the z components of the wave vector and are calculated from $k_{z_1}^2 = \varepsilon_{in} k_0^2 - \beta(\omega)^2$ and $k_{z_2}^2 = \varepsilon_m k_0^2 - \beta(\omega)^2$, where ε_{in} and ε_m are the dielectric constant of the insulator and metal, respectively, $k_0 = \frac{2\pi}{\lambda}$ is the free space wave number, H indicates the width of the insulator medium, ω is the operational radial frequency, and ε_0 is the permittivity of vacuum. The propagation constant β is described by the effective refractive index n_{eff} as $\beta = k_0 n_{eff}$. Fig. 1(b) displays the simulation of transmittance and reflectance of the structure shown in Fig. 1(a). The physical parameters were chosen to be $W = 60$ nm as the width of the input port, $W_t = 60$ nm is the width of the stub, $W_{gap} = 130$ nm is the distance between each two stubs, $d = 400$ nm is the length of stub, $D = d +$

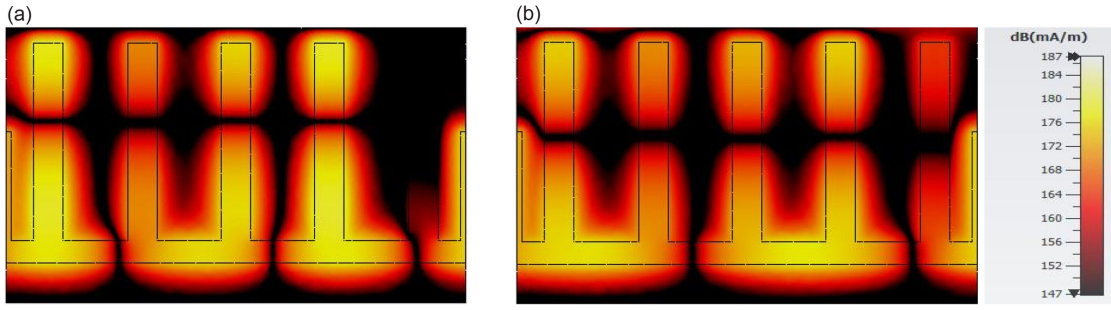

Fig. 2. Map of magnitude of the magnetic field distributions of the dual band-pass filter with W = 225 nm, H = W_t = 60 nm, d = 400 nm, D = d+H = 460 nm, W_{gap} = 130 nm, ∧ = W_{gap}+ W_t = 190 nm, W_r = 10 nm, L_r = 180 nm and G_r = 45 nm, at resonance wavelengths of (a) 1310 nm, and (b) 1550 nm.

H = 460 nm as the length from the bus waveguide to the end of the stub's length. The transmission and reflection profile demonstrated in Fig. 1(b) resembles that of a high-pass filter.

The main focus of the study has been to provide wavelength filtering functionality at the technologically significant optical channels, specifically O-band and C- band. Accordingly, two stepped-like apertures have been linked to input and output ports of the MIM waveguide, in order to contribute to resonance peaks at telecom wavelengths. The proposed structure of the multipurpose plasmonic wavelength filter is demonstrated in Fig. 1(c). Fig. 1(d) denotes transmission and reflection spectrum as a function of wavelength of the MIM plasmonic waveguide for W = 225 nm, 245 nm and 265 nm, W_t = 60 nm, W_{gap} = 130 nm, d = 400, D = d + H = 460 nm, with the stepped-like apertures' parameters chosen to be W_r = 10 nm, L_r = 180 nm, and G_r = 45 nm as the width, length and the coupling distance between the stepped-like apertures' and stubs, respectively. It is clear that the contribution of the reflectors, and the subsequent optimization of the length and the width of the stepped-like apertures, resulted in two resonance peaks at the desired telecom wavelengths of 1310 nm and 1550 nm, possessing 80.11% and 81.96% efficiencies, respectively. Moreover, the reflectance at resonance wavelengths are 0.010 and 0.009, respectively, that proves the excellent performance of stepped-like apertures in the structure at the pass bands and consequently, forming reflectance at undesired wavelengths between the two pass bands. It is worth citing that we have conducted comprehensive studies regarding the most suitable values for the MIM waveguide and thus, all values are achieved for the best performance in terms of resonance wavelengths positions, minimizing the size of the structure, while contributing to reduction of the loss in the device. However, we have realized that there is a trade-off between performance and loss in the plasmonic device. Interestingly, it is found that decreasing the width of the input port does neither cause red-shift nor blue-shift. The quality factor is defined as Q = $\frac{\lambda_{res}}{FWHM}$ and is mainly characterized by intrinsic loss in plasmonic devices, that is the ratio of the energy stored in the cavity at resonance to the energy lost per cycle of oscillation. So, the quality factor is attained by dividing the resonance wavelength by full width at half maximum (FWHM), and are 16.35 and 17.07, respectively.

From a physics point of view, the stub resonator structure form typical Fabry-Perot (FP) cavities, and the SPPs are reflected backwards and forwards within the waveguide due to the coupling between stepped-like apertures, stubs, and the bus waveguide, causing constructive interference within the waveguide structure. The magnitude of the magnetic field distribution at the resonance peak wavelengths of 1310 nm and 1550 nm are shown in Fig. 2(a)–(b), indicating that electromagnetic waves propagate in the structure and generate standing waves due to the horizontally and vertically reflected SPPs at the metal-insulator interface. The phase shift brought to the light wave, as a result of a single reflection, can be written as:

$$\varphi = \frac{4\pi \, \mathrm{Re}\,(n_{eff})\, d}{\lambda} + \theta \tag{1}$$

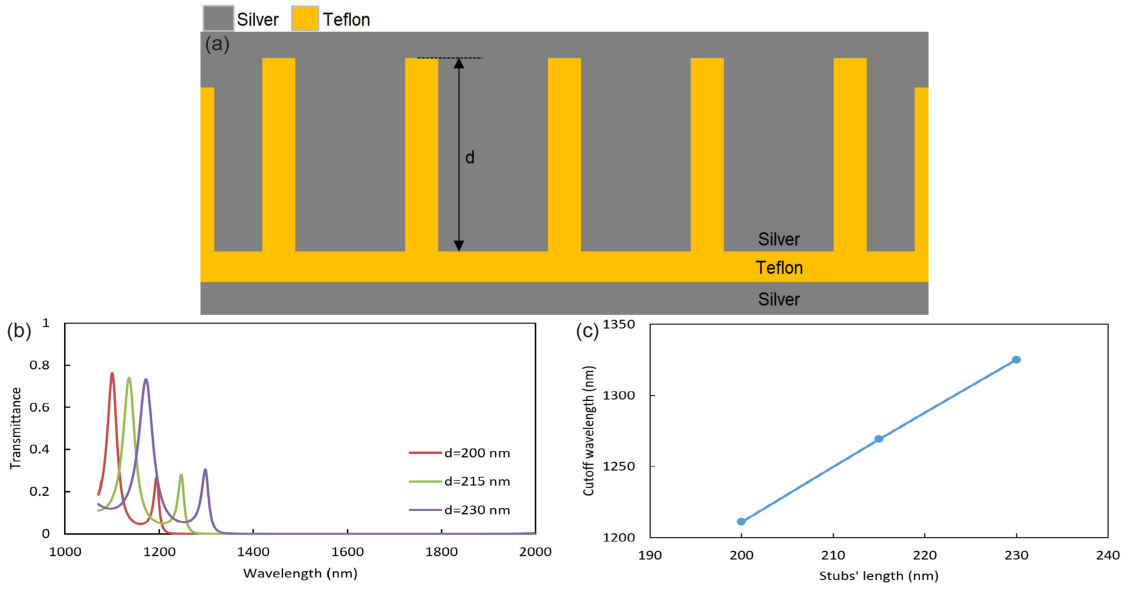

Fig. 3. (a) Schematic configuration of the cutoff wavelength filter; (b) Simulated spectra of the transmission profile for various lengths of stubs. (c) The relationship between the cutoff wavelengths and the lengths of the stubs.

where θ is the phase shift arising from the reflection at the metal-insulator interface. This phenomenon establishes the phase shift between a light wave propagating along the stubs and a light wave propagating along the bus waveguide, and the total phase shift between the two can be determined by [13]:

$$\varphi_{\text{total}} = \text{m}\left(\frac{4\pi\,\text{Re}\,(\text{n}_{\text{eff}})\,\text{d}}{\lambda} + \theta\right) \tag{2}$$

where m is the number of stubs travelled by the former light wave. For a perfect reflector,$\theta = \pi$. We define the accumulated phase shift per round trip in Fig. 1(c), as $\varphi = \varphi_{\text{total}} + \text{a}(\frac{4\pi\,\text{Re}(\text{n}_{\text{eff}})\text{L}_{\text{r}}}{\lambda} + \theta)$, where a is the number of stepped-like apertures. From Eq. (2), it is clear that the total phase shift of the structure is dependent on the length of the stub, as well as the effective refractive index. Finally, it should be pointed out that an accurate transmission function could be achieved for the proposed multifunctional plasmonic wavelength filter either by employing transmission line model (TLM) [26], or coupled mode theory (CMT) [27].

3. Results and Discussion

We systemically investigate the effect of structural parameters on the performance of the proposed multipurpose plasmonic filter. Fig. 3(a) exhibits a modified structure, in which the length of the stubs, d, has been reduced to half of its initial value. In Fig. 3(b), the transmission spectra of the plasmonic filter with different lengths of stubs (d = 200 nm, 215 nm and 230 nm, with all other parameters kept the same as in Fig. 1(c) are depicted. The response indicates the performance of a typical long-wavelength cutoff filter. The cutoff wavelength, defined as the wavelength where the transmission is equal to 1% [28], is found to be 1268.3 nm. Moreover, the modulation of the transmission spectrum is easily achieved by adjusting the length of the stubs. Fig. 3(c) demonstrates that the cutoff wavelength is a linear function of the length of the stubs, and can therefore easily

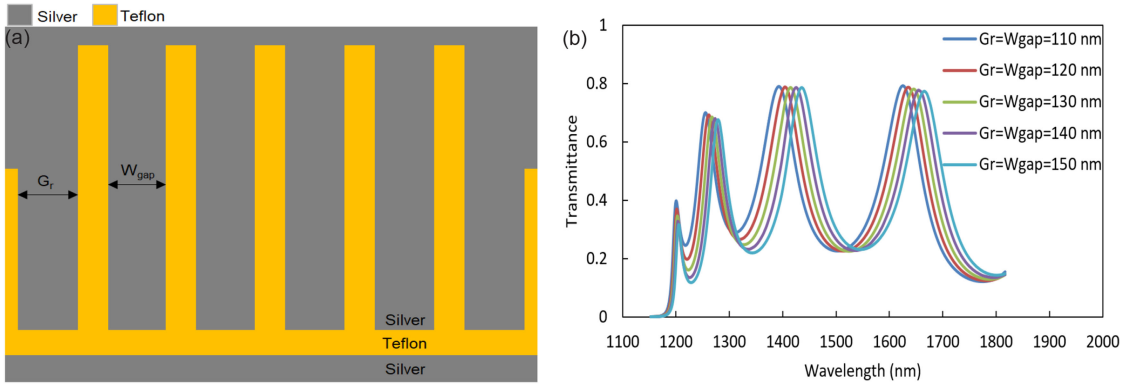

Fig. 4. (a) Schematic of the triple band-pass plasmonic filter, (b)Simulation results of transmission profile for different values of $G_r = W_{gap}$ = 110 nm,120 nm, 130 nm,140 nm, and 150 nm.

be tuned by varying the length of the stubs. It should be mentioned that the suggested broadband cutoff plasmonic wavelength filter operates over a wide range of frequency.

To further investigate the impact of the stepped-like apertures on the proposed plasmonic wavelength filter's transmission spectrum, the coupling distance between the stepped-like apertures and the corresponding adjacent stubs are modified, as shown in Fig. 4(a). In fact, we set the distance to $G_r = W_{gap}$ = 110 nm,120 nm,130 nm,140 nm, and 150 nm. The transmission spectra are presented in Fig. 4(b), where, to the best of our knowledge, for the first time a triple band-pass filter is demonstrated at telecom wavelengths based on plasmonics, only.

For example, when the coupling distance is chosen to be $G_r = W_{gap}$ = 130 nm, i.e., the distance between stepped-like apertures and nearby stubs are set to be identical to the distance between two neighboring stubs, there will be three resonance peaks in the transmission spectrum. The transmission profile demonstrates three pass bands at the optical wavelengths 1267.5 nm, 1414.19 nm, and 1644.7 nm with efficiencies of 68.5%, 78.6% and 78.1%, respectively. The calculated Q-factor for the pass bands are 26.04, 15.88, and 17.01, respectively. In addition to that, it is worth noting that in wavelength division multiplexing (WDM) systems with broad applications in optical signal processing, it is essential to separately select several particular wavelengths in various channels. Accordingly, multichannel filters such as the one presented in this paper, can play a fundamental role and may provide a promising concept for realization of miniaturized optical components in highly integrated optical circuits.

Next, Fig. 5(a) shows the schematic configuration of the plasmonic filter, in which tailoring the stepped-like apertures' lengths, stubs' length as well as the width of the bus waveguide make the device functioning as a broadband high-pass wavelength filter. We have here chosen the lengths of the stepped-like apertures and the stubs to be identical. The transmission spectra as a function of wavelength for $L_r = d$ = 40 nm, 50 nm, 60 nm and 70 nm are displayed in Fig. 5(b), whereas other parameters are the same as in Fig. 1(c).

The high-pass wavelength, corresponding to a transmission of 1%, is located at 800 nm. It is evident that the efficiency of the transmission for different values of L_r and d is over 82%. The broadband high-pass filter covers near-infrared (NIR) range up to the wavelength of 2 μm. Finally, we will conduct an investigation regarding the influence of the width of the stubs on the transmission spectrum. In Fig. 6(a), the widths of the stubs are chosen to be W_t = 10 nm, 16.8 nm, 20 nm, 30 nm and 40 nm, while all other structural parameters are kept the same as in Fig. 1(c). The absorption parameter, which describes the loss in the structure, is defined as $A = 1 - R - T$. It can be seen that the proposed structure is acting as a narrow-band nearly perfect absorber. The numerical results for different widths of the stubs are shown in Fig. 6(b). Furthermore, the suitable absorption

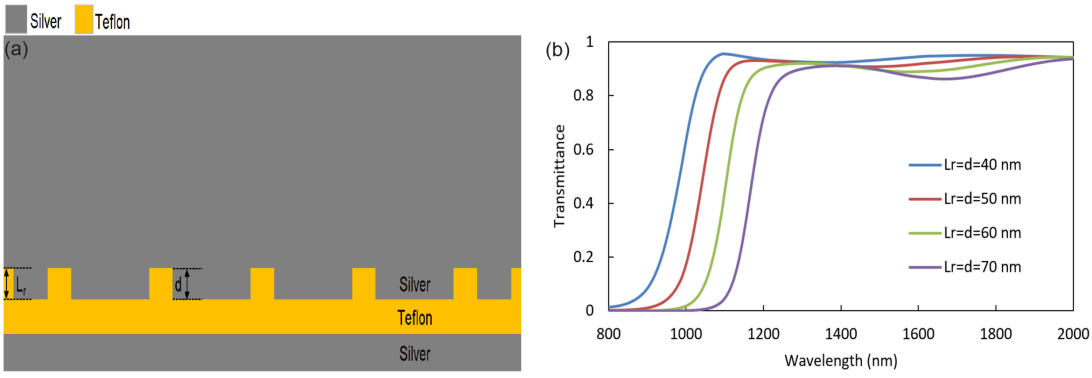

Fig. 5. (a) Schematic of the high-pass wavelength filter; (b) Simulated transmission spectra as a function of wavelength for different values of $L_r = d = 40$ nm, 50 nm, 60 nm and 70 nm.

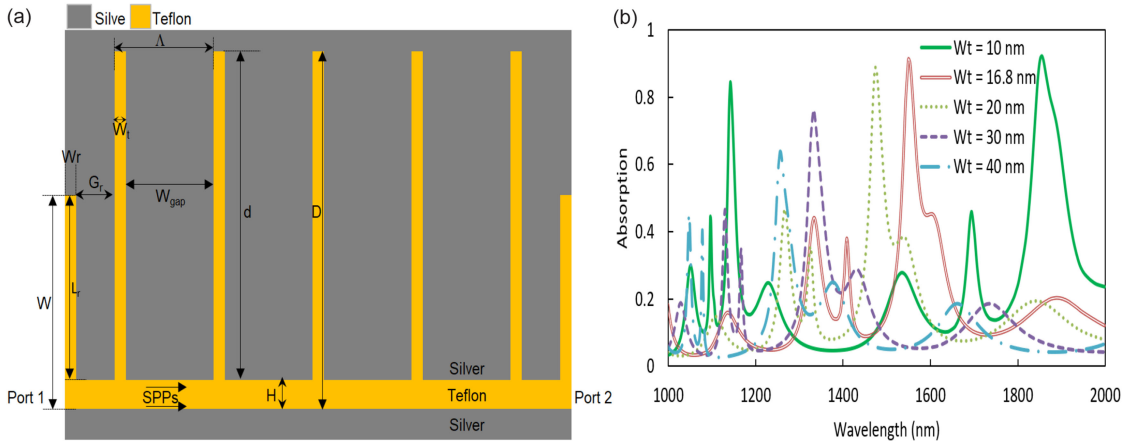

Fig. 6. (a) Schematic structure of suggested proposed nearly perfect absorber; (b) Simulation of absorption spectra for different stubs' widths as $W_t = 10$ nm, 16.8 nm, 20 nm, 30 nm and 40 nm.

peak can be easily attained by tailoring the width of the stubs. For instance, for $W_t = 16.8$ nm it is found that the absorption peak is around the wavelength of 1550 nm with an efficiency of more than 91.4%.

Clearly, the reason behind the formation of loss in the structure in this configuration is largely due to the rise of the surface plasmons. Indeed, the variation in the stubs' widths has contributed to the introduction of a peak in the absorption spectra as depicted in Fig. 6(b). This is because most of the incident light is trapped in the stub resonators and causes occurrence of reflection suppression in the plasmonic waveguide structure near the resonance wavelengths. The proposed plasmonic absorber may find applications in photovoltaics. Besides, the performance of the multipurpose plasmonic filter presented here has a higher efficiency and a smaller size, as compared to recent research studies and is illustrated in Table 1. Therefore, it holds a great potential in the path towards the realization of compact optical integrated circuits. In terms of the fabrication process, a modified laser interference lithography (LIL) method was recently suggested to alleviate degradation in the filtering performance, thereby provide grounding for manufacturing of large-area plasmonic filters [33], although the small size of the stepped-like apertures presented in this paper provides a challenge in the manufacturing operation.

TABLE 1
Comparison of Filters' Performance Between This Work and Previously Published Papers

Reference	Functionality	size	Resonance Peak	Efficiency	Publication Year
[29]	Band-pass	~1050 nm × 1700 nm	732 nm and 1174 nm	70% and 37%	2018
[30]	Band-pass	~1000 nm × 960 nm	640 nm and 1001 nm	44% and 51%	2019
[31]	Band-pass	~2000 nm × 400 nm	1305 nm and 1613 nm	75 % and 82%	2013
[32]	Band-pass	~1250 nm × 750 nm	960 nm and 1310 nm	66% and 68%	2019
This work	Band-pass	930 nm × 765 nm	1310 nm and 1550 nm	80.11% and 81.96%	2020
This work	Band-pass	1100 nm × 765 nm	1267.5 nm, 1414.19 nm, and 1644.7 nm	68.5%, 78.6%, and 78.1%	2020

4. Conclusion

In summary, a multipurpose and ultra-compact plasmonic wavelength filter based on MIM waveguides is proposed and the transmission characteristics of the device is numerically analyzed. The numerical results demonstrated that a dual band-pass filter at the technologically important telecom wavelengths at O- and C-bands can be achieved. In addition to that, variation of structural parameters on the transmission profile of the filter is investigated and shown to yield functionalities such as a long wavelength cutoff, a triple band-pass, and a high-pass filter, as well as a narrow-band nearly perfect absorber. As a result, the novel plasmonic wavelength filter may find application in optical communication systems. Moreover, the main reason for utilizing a stub-based device for wavelength filtering operations is its ability to reduce the size of optical components by using a simple structure in combination with the ease of manufacturing such structures. We therefore anticipate that our work may contribute to the emergence of a new class of nanostructures which are multipurpose and highly efficient, that would-with progress in manufacturing processes - leads to the development and integration of multipurpose circuits into next generation of PICs.

Acknowledgment

The authors would like to thank Mr. Seyed Ali Ebadi for his continuous support and encouragement, and gratefully acknowledge fruitful discussion with Professor Max Yan from The Royal Institute of Technology (KTH).

References

[1] W. L. Barnes, A. Dereux, and T. W. Ebbesen, "Surface plasmon subwavelength optics," *Nature*, vol. 424, no. 6950, pp. 824–830, Aug. 2003.
[2] E. Ozbay, "Plasmonics: Merging photonics and electronics at nanoscale dimensions," *Science*, vol. 311, no. 5758, pp. 189–193, Jan. 2006.

[3] J. A. Schuller, E. S. Barnard, W. Cai, Y. C. Jun, J. S. White, and M. L. Brongersma, "Plasmonics for extreme light concentration and manipulation," *Nat Mater*, vol. 9, no. 3, pp. 193–204, Mar. 2010.
[4] C. Li, S. Li, Y. Wang, R. Jiao, L. Wang, and L. Yu, "Multiple Fano resonances based on plasmonic resonator system with end-coupled cavities for high-performance nanosensor," *IEEE Photon. J.*, vol. 9, no. 6, Dec. 2017, Art. no. 4801509.
[5] M. S. Islam *et al.*, "Localized surface plasmon resonance biosensor: An improved technique for SERS response intensification," *Opt. Lett.*, vol. 44, no. 5, pp. 1134–1137, Mar. 2019.
[6] M. Burla *et al.*, "500 GHz plasmonic mach-zehnder modulator enabling sub-THz microwave photonics," *APL Photon.*, vol. 4, no. 5, 2019, Art. no. 056106.
[7] I. V. Dzedolik and S. Skachkov, "Field-effect transistor based on surface plasmon polaritons," *J. Opt. Soc. Amer. A*, vol. 36, no. 5, pp. 775–781, May 2019.
[8] Z. Gao, F. Gao, and B. Zhang, "Multi-directional plasmonic surface-wave splitters with full bandwidth isolation," *Appl. Phys. Lett.*, vol. 108, no. 11, 2016, Art. no. 111107.
[9] Y. Chen, J. Dai, M. Yan, and M. Qiu, "Honeycomb-lattice plasmonic absorbers at NIR: anomalous high-order resonance," *Opt. Exp.*, vol. 21, no. 18, pp. 20873–20879, 2013.
[10] F. Taghian, V. Ahmadi, and L. Yousefi, "Enhanced thin solar cells using optical nano-antenna induced hybrid plasmonic travelling-wave," *J. Lightw. Technol.*, vol. 34, no. 4, pp. 1267–1273, Feb. 2016.
[11] J. Dionne, L. Sweatlock, H. Atwater, and A. Polman, "Plasmon slot waveguides: Towards chip-scale propagation with subwavelength-scale localization," *Physical Rev. B*, vol. 73, no. 3, 2006, Art. no. 035407.
[12] H. Li and R.-Z. Jiao, "Plasmonic band-stop filters based on tooth structure," *Opt. Commun.*, vol. 439, pp. 201–205, 2019.
[13] H. Wang *et al.*, "Tunable band-stop plasmonic waveguide filter with symmetrical multiple-teeth-shaped structure," *Opt. Lett.*, vol. 41, no. 6, pp. 1233–1236, Mar. 2016.
[14] M. Zheng, H. Li, H. Xu, Z. He, Z. Chen, and M. Zhao, "Filtering property based on ultra-wide stopband in double sector/sectorial-ring stub resonator coupled to plasmonic waveguide," *IEEE Photon. J.*, vol. 9, no. 5, Oct. 2017, Art. no. 2201308.
[15] D. Liu, J. Wang, F. Zhang, Y. Pan, J. Lu, and X. Ni, "Tunable plasmonic band-pass filter with dual side-coupled circular ring resonators," *Sensors (Basel)*, vol. 17, no. 3, p. 585, Mar. 2017.
[16] L. Yang, Y. J. Zhou, C. Zhang, and Q. X. Xiao, "Compact wideband plasmonic filter with flat-top transmission response based on corrugated metal-insulator-metal ring resonator," *Scientific Rep.*, vol. 7, no. 1, 2017, Art. no. 14237.
[17] S. M. Ebadi and S. B. Ram, "A dual band-pass plasmonic filter based on stub structure in a MIM waveguide at optical channels," in *Proc. IEEE Photon. North*, 2015, p. 1.
[18] S. M. Ebadi, S. S. Sajjadi, M. S. Bayati, and S. B. Ram, "A tunable wavelength band pass plasmonic filter based on triangular arrays in a MIM waveguide," in *Proc. IEEE Photon. North*, 2015, p. 1.
[19] M. A. Bavil, L. Gao, and X. Sun, "A compact nanoplasmonics filter and intersection structure based on utilizing a slot cavity and a fabry–perot resonator," *Plasmonics*, vol. 8, no. 2, pp. 631–636, 2013.
[20] Y. Feng *et al.*, "Compact nanofilters based on plasmonics waveguide with archimedes' spiral nanostructure," *IEEE Photon. J.*, vol. 8, no. 5, Oct. 2016, Art. no. 4802908.
[21] D. Pérez, I. Gasulla, and J. Capmany, "Programmable multifunctional integrated nanophotonics," *Nanophotonics*, vol. 7, no. 8, pp. 1351–1371.
[22] T. Zhuang, S. Li, G. Song, P. Jiang, and L. Yu, "Tunable band-stop plasmonic waveguide filter with single-sided multiple-teeth-shaped structure," *Physica Scripta*, vol. 94, no. 9, p. 095602, 2019.
[23] P. B. Johnson and R.-W. Christy, "Optical constants of the noble metals," *Physical Rev. B*, vol. 6, no. 12, 1972, Art. no. 4370.
[24] C.-C. Cho, D. Smith, and J. Anderson, "Low dielectric-constant insulators for electronics applications," *Mater. Chemistry Phys.*, vol. 42, no. 2, pp. 91–95, 1995.
[25] N. H. T. Tran *et al.*, "Dielectric metal-based multilayers for surface plasmon resonance with enhanced quality factor of the plasmonic waves," *J. Electron. Mater.*, vol. 46, no. 6, pp. 3654–3659, 2017.
[26] A. Pannipitiya *et al.*, "Improved transmission model for metal-dielectric-metal plasmonic waveguides with stub structure," *Opt. Exp.*, vol. 18, no. 6, pp. 6191–6204, 2010.
[27] Q. Li *et al.*, "Coupled mode theory analysis of mode-splitting in coupled cavity system," *Opt. Express*, vol. 18, no. 8, pp. 8367–8382, 2010.
[28] S. M. Ebadi, M. S. Bayati, S. B. Ram, S. M. Poursajadi, and M. Jamili, "High-efficiency nanoplasmonic wavelength filters based on MIM waveguides," *IEEE Photon. Technol. Lett.*, vol. 28, no. 22, pp. 2605–2608, Nov. 2016.
[29] S. Khani, M. Danaie, and P. Rezaei, "Realization of single-mode plasmonic bandpass filters using improved nanodisk resonators," *Opt. Commun.*, vol. 420, pp. 147–156, 2018.
[30] S. Khani, M. Danaie, and P. Rezaei, "Design of a single-mode plasmonic bandpass filter using a hexagonal resonator coupled to graded-stub waveguides," *Plasmonics*, vol. 14, no. 1, pp. 53–62, 2019.
[31] K. Thirupathaiah, N. P. Pathak, and V. Rastogi, "Concurrent dual band filters using plasmonic slot waveguide," *IEEE Photon. Technol. Lett.*, vol. 25, no. 22, pp. 2217–2220, Nov. 2013.
[32] M. R. Pav *et al.*, "Ultracompact double tunable two-channel plasmonic filter and 4-channel multi/demultiplexer design based on aperture-coupled plasmonic slot cavity," *Opt. Commun.*, vol. 437, pp. 285–289, 2019.
[33] Y. S. Do, "A highly reproducible fabrication process for large-area plasmonic filters for optical applications," *IEEE Access*, vol. 6, pp. 68961–68967, 2018.